LA-UR- 09-00931

Approved for public release;
distribution is unlimited.

Title:	Measurement of Porosity in a Composite High Explosive as a Function of Pressing Conditions by Ultra-Small-Angle Neutron Scattering with Contrast Variation
Author(s):	Joseph T. Mang, Rex P. Hjelm and Elizabeth G. Francois
Intended for:	Propellants, Explosives, Pyrotechnics

Los Alamos
NATIONAL LABORATORY
EST. 1943

Form 836 (7/06)

Measurement of Porosity in a Composite High Explosive as a Function of Pressing Conditions by Ultra-Small-Angle Neutron Scattering with Contrast Variation

Joseph T. Mang, Rex P. Hjelm and Elizabeth G. Francois

Los Alamos National Laboratory, Los Alamos, NM 87545

February 12, 2009

Abstract

We have used ultra-small-angle neutron scattering (USANS) with *contrast variation* to measure the porosity (voids and binder-filled regions) in a composite high explosive, PBX 9501, formulated with a deuterated binder. Little is known about the microstructure of pressed PBX 9501 parts and thus how it is affected by processing. Here, we explore the effect of varying the pressing intensity on the PBX 9501 microstructure. Disk-shaped samples of PBX 9501 were die-pressed with applied pressures ranging between 10,000 and 29,000 psi at 90°C. Five samples were prepared at each pressure that differed in the fraction of deuterated binder, facilitating variation of the neutron scattering length density contrast ($\Delta\rho$) and thus, the resolution of microstructural details. The sample composition was determined by calculation of the Porod Invariant as a function of $\Delta\rho$ and compared with compositional estimates obtained from the bulk sample density. Structural modeling of the USANS data, at different levels of contrast, assuming both spherical and cylindrical morphologies, allowed the mean size and size distribution of voids and binder-filled regions to be determined. A decrease in the mean diameter of binder-filled regions was found with increasing pressing intensity, while the mean void diameter showed no significant change.

Introduction

High explosive (HE) materials are commonly composites of crystalline high explosives and a polymeric binder. The polymeric binder imparts both structural integrity and plasticity to the HE, allowing it to be readily pressed to specific densities. The binder can also affect HE performance and sensitivity by influencing the propagation of microstresses between the crystalline grains under shock and loading conditions[1]. The presence of intergranular voids in a pressed HE can affect the material's response to certain stimuli by creating locally heated regions or *hot spots* and are of great interest from both safety and performance perspectives[2]. The critical hot spot temperature is dependent upon a number of variables, including the size of the defect. In general, void sizes greater than 0.2 μm in diameter are thought to be the most influential in hot spot formation. The void fraction, ϕ_v, in a pressed piece of HE is defined as,

$$\phi_V = 1 - \frac{d}{d_{TMD}}, \qquad (1)$$

where, d is the pressed density and d_{TMD} is the theoretical maximum density (TMD) of the high explosive.

Understanding the relationship between sensitivity and pressed density of HE has been of interest for many years[3-5]. Campbell[3] found that the sensitivity of plastic bonded HMX decreased rapidly with increasing pressed density (or decreasing void fraction). Lee[4] and co-workers showed an increase in the impact velocity threshold for initiation with increasing pressed density for several different formulations of the high explosive, TATB. The increased threshold was associated with a decrease in the average diameter of intergranular pores.

In order to better understand safety and sensitivity tests and to advance the predictive capabilities of HE performance, an accurate measure of the intergranular pore (voids and binder-filled) size distribution in an explosive is needed. Such a measurement has proven to be difficult. Porosity in pressed neat (no binder) high explosives has been measured by Mercury intrusion[4]. However questions over the accessibility of the mercury to *closed porosity* (pores or voids which are not open to the surface) have obscured the meaning of the measured pore volume. This difficulty is exacerbated with the addition of a polymer binder. Additionally, the high pressures involved in Mercury intrusion measurements have the potential to alter the original pore size distribution.

Small-angle scattering techniques employing x-rays and neutrons are commonly used to measure porosity in materials and can provide a quantitative measure of pore size and size distribution[6-11]. The penetrating nature of x-rays and neutrons allows the entire sample volume to be probed, so that both *open* and *closed* porosity can be measured, making the techniques applicable to HE systems[5,9-11]. Neutron scattering techniques, such as ultra-small-angle neutron scattering (USANS) have unique applicability to composite systems. By exploiting the difference, through contrast variation, in which hydrogen and deuterium scatter neutrons, USANS can distinguish between voids and binder-filled regions in a composite high explosive, thus providing a new level of microstructural detail that may further the understanding of HE sensitivity and performance. USANS instruments[12] can quantify pores having radii in the range 0.005 – 10 μm, length scales that are of greater interest to HE performance and sensitivity. Recently, ultra-small-angle x-ray scattering (USAXS) measurements of voids on the order of 1 μm were reported on a different composite HE system[11].

PBX 9501 is a composite high explosive with a TMD of 1.86 g/cm^3, consisting of a bimodal distribution (3:1, coarse:fine) of HMX (94.9 wt %), a polymeric binder (5.0 wt %, Estane + nitroplasticizer) plus a small amount (0.1 wt %) of stabilizer. PBX 9501, like other HE systems, possesses both naturally occurring and process-related defects (cracks, voids, etc.), which have the potential to dramatically affect its ignition sensitivity and performance. While these features can be characterized in the raw material, little is known about the composite or how they are affected during processing.

During the preparation of PBX 9501 parts, variables such as pressing intensity, temperature, number of pressing cycles, dwell time, and rest time (between cycles) are varied in order to achieve nominal density. Although bulk density is met, differences in pressing conditions can lead to variations in microstructure, which can lead to variations in mechanical properties, and hence response, between parts. Thompson and co-workers recently reported that pressing conditions can be tuned to achieve the desired mechanical properties of a composite HE[13].

In order to understand how the variation of pressing intensity affects its microstructure, we have employed USANS with contrast variation to measure the mean size and size distribution of voids and binder-filled regions in PBX 9501. The USANS data from PBX 9501 were analyzed as a three phase system (HMX crystals, voids and binder-filled regions) as each component contributes to the total scattering signal. The unique ability to vary the scattering length density contrast, along with the development of structural models, allowed deconvolution of the USANS scattering signal and quantification of structures in the different phases.

USANS Analysis

The scattered intensity, I(Q), observed in a USANS experiment is directly related to the structure of the sample through the squared Fourier transform of the scattering length density, $\rho(\mathbf{r})$. Scattering derives from fluctuations in $\rho(\mathbf{r})$, which reflects microscale structure in the sample density and in the chemical and isotopic composition. Scattering intensity is measured in the absolute units of differential cross section per unit volume, I(Q) (cm^{-1}) as a function of scattering vector, **Q**, of magnitude $Q = (4\pi/\lambda)\sin\theta$, where λ is the wavelength of the incident neutron and θ is half of the scattering angle[14]. For a population of randomly oriented, non-interacting particles dispersed in a uniform medium (a two phase system), I(Q) can be expressed as,

$$I(Q) = \phi\overline{\Delta\rho}^2 \int_0^\infty f(R)V(R)\left\langle |F(\boldsymbol{Q},R)|^2 \right\rangle dR = \phi\overline{\Delta\rho}^2 P(Q), \qquad (2)$$

where $F(\boldsymbol{Q},R)$ is the normalized Fourier transform of $\rho(\mathbf{r})$ and contains information about the particle shape. $f(R)$ is the probability of finding a particle having a radius between R and $R + dR$, $V(R)$ is the particle volume, and ϕ is the volume fraction of scatterers[14]. The brackets indicate a spherical average over particle orientation. $\overline{\Delta\rho}$ is the average scattering length density contrast between the average scattering length density of the particle, and that of the surrounding media. Common forms of the form factor, $\left\langle |F(\boldsymbol{Q},R)|^2 \right\rangle$, are, for a uniform spherical particle of radius, R,[14]

$$\left\langle |F(\boldsymbol{Q},R)|^2 \right\rangle = 9\left[\frac{\sin(QR - QR\cos(QR)}{Q^3R^3}\right]^2, \qquad (3)$$

and, for a uniform cylindrically symmetric particles of radius, r, and length, L,

$$\left\langle \left|F(\boldsymbol{Q},R)\right|^2 \right\rangle = 16\int_0^{\frac{\pi}{2}} \left| \frac{\sin(QL\cos\beta)}{QL\cos\beta} \frac{J_1(Qr\sin\beta)}{Qr\sin\beta} \right|^2 \sin\beta d\beta, \quad (4)$$

where J_1 is the first order Bessel function and β is the angle of orientation.

Using the equation derived by Wu[15] to describe the scattering from a three phase composite, the neutron scattering from PBX 9501 can be expressed as,

$$I(Q) = (\rho_b - \rho_h)(\rho_v - \rho_h)\phi_h(1-\phi_h)P_h(Q) + (\rho_v - \rho_b)(\rho_h - \rho_b)\phi_b(1-\phi_b)P_b(Q) + (\rho_h - \rho_v)(\rho_b - \rho_v)\phi_v(1-\phi_v)P_v(Q). \quad (5)$$

Here, *h*, *b*, *v* represent the HMX, binder and void phases, respectively, and $P_i(Q)$ is as defined in Eq. 2 and represents the scattering from an individual phase. Eq. 5 can be simplified using the well known Babinet[14] principle to express the scattering from the HMX phase in terms of the binder and void phases:

$$P_h(Q) = \frac{\phi_b P_b(Q) + \phi_v P_v(Q)}{\phi_b + \phi_v}.$$

The Porod Invariant, Q_p, is a useful quantity which, for particles of known scattering length density, allows a model independent determination of the sample composition from the scattering data. The Porod Invariant is given by[14,15],

$$Q_p = \int_0^\infty Q^2 I(Q) dQ, \quad (6a)$$

and for the three phase, PBX 9501 system[15],

$$Q_p(\rho_b) = 2\pi^2\left[(\rho_h - \rho_b)^2\phi_h\phi_b + (\rho_b - \rho_v)^2\phi_b\phi_v + (\rho_v - \rho_h)^2\phi_v\phi_h\right]. \quad (6b)$$

Contrast variation was used, in conjunction with analysis according to Eqs. 5-6, to deconvolute the scattering signals from the three phases of PBX 9501. With this method, $\Delta\rho$ is systematically varied with the introduction of a deuterated fluid or the isotopic

substitution of deuterium for hydrogen in one of the components. Deuterium has a very different scattering length than hydrogen, so by varying the amount of deuterium present, different structural features can be emphasized (or deemphasized)[9,14].

For the present analysis, $\Delta\rho$ was varied by formulating the PBX 9501 with different amounts of deuterated binder, while keeping the total fraction of the binder constant. USANS data were analyzed according to Eq. 5 by simultaneously fitting a structural model to the data at five different contrasts, using the non-linear least squares method of Marquardt[16]. Size distributions for void and binder-filled regions were obtained for both spherical and cylindrical form factors (Eqs. 3 and 4) and a lognormal probability distribution function (*f(R)* in Eq. 2).

$\underline{Q_p}$ (Eq. 6a) was calculated from the USANS data at each contrast and then fit according to Eq. 6b, enabling the components volume fractions to be determined.

Experimental

PBX 9501 was formulated at Los Alamos National Laboratory, with a deuterated binder. The binder is a 50/50 mixture (by weight) of a polymer (Estane®) and a plasticizer (BDNPA/F). For these experiments, both the polymer and plasticizer were replaced with deuterated analogs. Five different formulations were prepared, each with a different amount of deuterated binder (0-100%, in 25% increments). The neutron scattering length densities of the PBX 9501 components are listed in Table I.

The different formulations were prepared in 10g batches. For each batch, a lacquer was made with the binder(s) and plasticizer(s) dissolved in 20ml of methyl ethyl ketone (MEK) with one hour of shaking. The lacquer was added to the HMX and hand

mixed until it appeared homogenous and near dry and then placed in a vacuum oven and dried at 60°C overnight.

The resulting formulations were die-pressed, at 90°C with applied pressures ranging between 10 kpsi and 29 kpsi, into disks 9.5 mm in diameter and 1 mm thick. Two 30 s intensifications were used with a 30 s rest period in between. Five disks, each with a different level of deuteration, were prepared under each pressing condition in order to vary $\Delta\rho$. The average density, void volume fraction and pressing conditions of the samples are summarized in Table II. There is no significant difference in the average bulk density among the three sample sets (Table II).

USANS measurements were performed at the National Institute of Standards and Technology Center for Neutron Research (NCNR) using the BT-5[12] Perfect Crystal SANS instrument and a monochromatic neutron wavelength of 2.4 Å. The samples were sealed inside rectangular cells made of fused silica. The BT-5 instrument is a Bonse-Hart[12] camera with a maximum effective Q-range of 0.00003 – 0.01 $Å^{-1}$ and size range from 0.1 – 20 μm.

USANS data were reduced by conventional methods and corrected for empty cell and background scattering. The data and model curves presented here are slit smeared (according to the instrument resolution) in order to avoid the potential of introducing artifacts in the desmearing process. Absolute intensities are reported as differential cross section per unit volume (cm^{-1}).

Results and Discussion

Figure 1 shows a plot of the Porod Invariant (Eq. 6a) calculated for the series of PBX 9501 samples pressed at 20 kpsi which is representative of the data obtained for the 10 and 29 kpsi samples. The data display the anticipated behavior as a function of the scattering length density of the binder. The solid line in the figure is a fit to Eq. 6b, that provides a model-independent measurement of the composition of the PBX 9501 microstructure (Table II). From this composition, the average density of each set of samples was calculated and is listed in Table II. As seen in the table, there is agreement between the average sample densities and compositions determined from the Porod Invariant analysis and the corresponding values obtained from the bulk properties of the samples.

Figure 2 shows a log-log plot of the USANS data obtained from five disks of PBX 9501, containing different fractions of deuterated binder, that were die pressed with an applied pressure of 29 kpsi . The data exhibit power law scattering (which appears linear on a log-log plot) at low- Q values, followed by a Guinier region. The Guinier region appears as a "knee" in the data and its position along the Q-axis is indicative of the mean size of the scattering objects. Power-law scattering is often interpreted as indicating a fractal-like structure of the scattering particles. However, highly polydisperse, non-fractal systems as well as asymmetric particles can exhibit power-law scattering. While an attempt has been made to describe the PBX 9501 microstructure in terms of fractals[17], much of the characterization performed, including USANS measurements of pressed pellets of HMX without binder[18], suggests that it is non-fractal[9,19,20]. Data obtained from

samples prepared with applied pressures of 20 and 10 kpsi show the same general features as those displayed in Fig. 2.

As seen in Fig. 2, the USANS intensity changed little with the increasing level of deuteration in the Q-range between 0.00003 and 0.0001 $Å^{-1}$, but significant changes were seen at higher Q-values. This suggests that the low-Q data is dominated by scattering from voids surrounded by the high explosive (HMX), which is independent of the binder deuteration level and that at higher Q-values, the scattering is dominated by the binder-filled regions. The position of the Guinier region, as seen in Fig. 2, changed with increasing deuteration of the binder, indicative of overlapping size regimes for the void and binder-filled regions.

We modeled the USANS data from PBX 9501 according to the three phase model of Wu[15] (Eq. 5), using both spherical (Eq. 3) and cylindrical (Eq. 4) form factors to describe the morphology of the polydisperse, voids and binder regions. In order to help constrain the model parameters, the data were simultaneously fit to Eq. 5 at different contrasts, leaving the deuteration level of the binder as the only variable among the data sets. During the spherical analysis, a sum of lognormal functions was chosen to represent $f(R)$ in Eq. 2, for both voids and binder particles. For the cylindrical analysis, the cylinder radius, r, was treated as monodisperse and thus represents an average value, while the distribution of cylinder lengths, $f(L)$, was represented by a sum of lognormal functions. Initial values of the volume fractions in Eq. 5 were set to those determined by analysis of $Q_p(\Delta\rho)$ (Eq. 6b, Table II), however the volume fraction parameters were allowed to vary during the spherical analysis in order to improve the quality of the fit. These fitted values of the volume fractions were fixed during the cylindrical analysis. The solid lines in Fig.

2 are the result of simultaneous fits, assuming a spherical shape for both the voids and binder regions and are indicative of the quality of the fits obtained for all samples. Analysis according to the cylindrical model is indistinguishable from the spherical analysis.

Plots of the volume-weighted size distributions of voids and binder regions, assuming a spherical morphology, are shown in figures 3 and 4, respectively, for the range of applied pressures. The void distributions are characterized by a primary mode between 0.66 and 0.70 μm, which decreases with increasing pressure. In contrast, the primary mode of the binder distributions (Fig. 4) increases and shifts to smaller diameters with increasing pressing intensity. The compositional information obtained from the model analysis can be found in Table II and the mean void diameter and mean diameter of the binder regions are listed in Table III.

The spherical model, while consistent with the bulk and Porod Invariant analysis, yielded a higher volume fraction of HMX and lower volume fractions for both the binder and void phases for the three pressing conditions (Table II), and thus, higher average sample densities (< 2%) in comparison to the other two techniques. No trend is observed for the mean void diameter with increasing pressing intensity, while the mean diameter of the binder-filled regions decreased monotonically (Table III) with increasing pressure. In contrast, the void volume fraction was found to decrease slightly as pressure increased, while no change in binder volume fraction was found (Table II).

With increasing pressure it can be anticipated that the binder will spread and coat the HMX surfaces more completely, thus filling some of the void volume. This can lead to a smaller average size of a binder region, while leaving the binder volume fraction

unchanged. The data suggests that the binder fills the smaller voids as the void volume decreases and there is no significant change in the mean void size. This notion is supported by the void volume distributions (Fig. 3), which show a significant decrease at smaller diameters.

In an attempt to better understand the morphology of the voids and binder-filled regions of the PBX 9501 microstructure, we repeated the three-phase model analysis assuming that both scattering regions have cylindrical symmetry, using the cylindrical form factor (Eq. 4) in place of the spherical form factor in Eq. 5. As discussed earlier, the USANS data displays power-law scattering (Fig. 2). For $Q < 0.0001$ Å^{-1}, the PBX 9501 data, regardless of the deuteration level, fall-off as a power-law with an exponent of ~ 1.3. For slit-smeared data, this is suggestive of short cylinders or a disk-like morphology. As seen in Table IV, the mean values of the model parameters are consistent with a disk-like structure ($D > L$) for both the voids and binder-filled regions, with the voids having an aspect ratio ($AR = D/L$) between 13 and 14 and the binder-filled regions having an AR between 5 and 6. Plots of the volume-weighted disk length distribution for the voids and binder-filled regions are shown in figures 5 and 6. The void distributions are characterized by a single mode, centered at $L \sim 0.25$ μm that decreases with increasing pressing intensity, similar to the primary mode of the spherical model (Fig. 3). Similarly, the volume-weighted disk length distributions for the binder-filled regions appear monomodal (Fig. 6.), with the peak shifting to smaller values as the pressing intensity increases, consistent with the spherical analysis.

Summary

USANS and contrast variation measurements have been used to measure the composition of, and the mean size and size distribution of voids and binder-filled regions in, the microstructure of PBX 9501 pressed at 90°C with applied pressures ranging from 10 kpsi to 29 kpsi, in order to understand how the processing conditions affect the final microstructure. There was no significant difference in the average density of the parts under investigation. The measurements are the first of their kind for PBX 9501 and were possible because of the unique capabilities of USANS to distinguish between scattering that arises from voids and binder. The morphological and size information presented can be implemented in microstructural modeling codes in order to better understand the detonation properties of PBX 9501.

The composition of the PBX 9501 microstructure was determined as a function of the applied pressure by Porod Invariant analysis and structural modeling of the USANS data. Both techniques were found to be consistent with bulk density estimates.

Structural modeling of the USANS data was performed, allowing the mean size and size distribution of voids and binder-filled regions to be determined. The mean diameter of the binder-filled regions, based upon the spherical model analysis, was found to decrease with increasing pressure, while the mean void diameter did not change appreciably. However, the volume fraction of voids decreased with increasing pressure, while the volume fraction of binder did not. This suggests that at the higher processing pressures, the binder spreads out and fills some of the smaller voids. Such a behavior should result in a larger surface area for the binder phase and will be the subject of a future small-angle neutron scattering (SANS) study.

Additional modeling of the USANS data was performed assuming a cylindrical symmetric morphology for the voids and binder-filled regions. The USANS data was consistent with a disk-like structure for both the voids and binder-filled regions, with the voids having an aspect ratio greater than two times that measured for the binder.

Future USANS measurements will build upon the techniques developed here as we plan to study the microstructure of PBX 9501 after subjection to thermal and mechanical insults.

Acknowledgements

The authors would like to thank E. Bruce Orler for supplying the deuterated binder materials, Stephanie Hagelberg and Ernie Hartline for pressing the PBX 9501 samples and John Barker for his help with the USANS measurements.

We acknowledge the support of the National Institute of Standards and Technology, U.S. Department of Commerce, in providing the neutron research facilities used in this work.

References

1 K. M. Roessig and J. C. Foster, in *Experimental Simulation of Dynamic Stress Bridging in Plastic Bonded Explosives*, 2001 (APS), p. 829-832.

2 C. Tarver, S. Chidester, and A. Nichols, J. Phys. Chem. **100,** 5794 (1996).

3 A. W. Campbell, W. C. Davis, J. B. Ramsay, and J. R. Travis, Physics of Fluids **4,** 511-521 (1961).

4 R. Lee, G. Bloom, W. von Holle, R. Weingart, L. Erickson, S. Sanders, C. Slettevold, and R. Mcguire, in *The Relationship Between the Shock Sensitivity and the Solid Pores Sizes of TATB Powders Pressed to Various Densities*, Albuquerque, NM July 15-19, 1985.

[5] C. B. Skidmore, D. S. Phillips, P. M. Howe, J. T. Mang, and J. A. Romero, in *The Evolution of Microstructural Changes in Pressed HMX Explosives*, Snowmass, CO, August 30-September 4, 1998.
[6] P. Fratzl, G. Vogl, and S. Klaumunzer, J. Appl. Cryst. **24,** 588 (1991).
[7] R. Hjelm, W. Wampler, P. Seeger, and M. Gerspacher, J. Mater. Res. **9,** 3210 (1994).
[8] K. Littrell, N. Khalili, M. Campbell, G. Sandi, and P. Thiyagarajan, Chem. Mater. **14,** 327 (2002).
[9] J. T. Mang, C. B. Skidmore, R. P. Hjelm, and P. M. Howe, J. Mater. Res. **15,** 1199-1208 (2000).
[10] P. Peterson, J. Mang, and B. Asay, J. Applied Phys. **97,** 093507 (2005).
[11] T. Willey, T. van Buuren, J. Lee, G. Overturf, J. Kinney, J. Handly, B. Weeks, and J. Ilavsky, Propellants, Explosives, Pyrotechnics **31,** 466-471 (2006).
[12] J. G. Barker, C. J. Glinka, J. J. Moyer, M. H. Kim, A. R. Drews, and M. Agamalian, Journal of Applied Crystallography **38,** 1004-1011 (1995).
[13] D. G. Thompson, B. Olinger, and R. Deluca, Propellants, Explosives, Pyrotechnics **30,** 391 (2005).
[14] O. Glatter and O. Kratky, *Small Angle X-ray Scattering* (Academic Press, London, 1982).
[15] W. Wu, Polymer **23,** 1907 (1982).
[16] D. W. Marquardt, J. Soc. Ind. Appl. Math. **2,** 431 (1963).
[17] J. M. McAfee, C. B. Skidmore, G. S. Cunningham, and R. A. Nelson, in *Explosive Morphology from Fractal Analysis of Micrographs*, Snowmass, CO, August 30-September 4, 1998.
[18] J. T. Mang, unpublished results.
[19] C. B. Skidmore, D. S. Phillips, S. F. Son, and B. W. Asay, in *Characterization of HMX Particles in PBX 9501*, Amherst, MA, 1997 (AIP), p. 579-582.
[20] N. J. Burnside, S. F. Son, B. W. Asay, and C. B. Skidmore, in *Particle Characterization of Pressed Granular HMX*, 1997 (AIP), p. 571-574.

Tables

Table I: Scattering length densities of PBX 9501 components

Component	ρ (x 10^{10} cm^{-2})
Void	0
HMX	4.50
Non-deuterated binder	1.99
25% deuterated binder	2.30
50% deuterated binder	2.61
75% deuterated binder	2.91
Fully deuterated binder	3.22

Table II: Volume fraction of HMX, binder and voids in PBX 9501 by different methods

Calculated From Bulk Density				
Pressing Conditions[†]	Average Density (g/cm^3)[£]	ϕ_{HMX}	ϕ_{binder}	ϕ_{voids}
10 kpsi	1.80 ± 0.03	0.90 ± 0.02	0.068 ± 0.001	0.03 ± 0.02
20 kpsi	1.82 ± 0.01	0.910 ± 0.005	0.068 ± 0.001	0.022 ± 0.005
29 kpsi	1.83 ± 0.01	0.915 ± 0.005	0.069 ± 0.001	0.016 ± 0.005
USANS - Porod Invariant				
10 kpsi	1.81 ± 0.02	0.909 ± 0.004	0.066 ± 0.005	0.025 ± 0.009
20 kpsi	1.82 ± 0.03	0.92 ± 0.01	0.06 ± 0.01	0.02 ± 0.02
29 kpsi	1.82 ± 0.03	0.92 ± 0.01	0.06 ± 0.01	0.02 ± 0.02
USANS - Three Phase Model (Spheres)				
10 kpsi	1.832 ± 0.002	0.930 ± 0.001	0.055 ± 0.001	0.015 ± 0.001
20 kpsi	1.840 ± 0.002	0.938 ± 0.001	0.051 ± 0.001	0.011 ± 0.001
29 kpsi	1.843 ± 0.002	0.936 ± 0.001	0.055 ± 0.001	0.009 ± 0.001

[†] Two 30s intensifications with 30s rest, die at 90° C
[£] TMD of PBX 9501 = 1.86 g/cm^3

Table III: Average Void and Binder Region Diameters from Spherical Analysis

Pressing Conditions[†]	Mean Void Diameter (μm)	Mean Binder Diameter (μm)
10 kpsi	2.40	0.79
20 kpsi	2.19	0.62
29 kpsi	2.36	0.59

[†] Two 30s intensifications with 30s rest, die at 90° C

Table IV: Average Void and Binder Region Dimensions from Cylindrical Analysis

Pressing Conditions[†]	Mean Void Diameter (μm)	Mean Void Length (μm)	Mean Binder Diameter (μm)	Mean Binder Length (μm)
10 kpsi	6	0.48	0.96	0.20
20 kpsi	6	0.43	0.91	0.16
29 kpsi	6	0.46	0.93	0.15

[†] Two 30s intensifications with 30s rest, die at 90° C

Figure Captions

Figure 1: Porod Invariant calculated for the series of PBX 9501 samples pressed at 20 kpsi. The solid line is a fit to Eq. 6b, that provides a model-independent measurement of the composition of the PBX 9501.

Figure 2: Log-log plot of the USANS data obtained from five disks of PBX 9501, containing different fractions of deuterated binder, that were pressed with an applied pressure of 29 kpsi. The solid lines are the result of simultaneous fits, assuming a spherical shape for both the voids and binder.

Figure 3: Volume-weighted size distributions of voids, assuming a spherical morphology, for the range of applied pressures. The void distributions are characterized by a primary mode between 0.66 and 0.70 μm, which decreases with increasing pressure.

Figure 4: Volume-weighted size distributions of binder-filled regions, assuming a spherical morphology, for the range of applied pressures. The distributions are characterized by a primary mode that increases and shifts to smaller diameters with increasing pressing intensity.

Figure 5: Volume-weighted disk length distributions for the voids, assuming a cylindrical morphology. The distributions are characterized by a single mode, centered at $L \sim 0.25$ μm that decreases with increasing pressing intensity.

Figure 6: Volume-weighted disk length distributions for the binder-filled regions, assuming a cylindrical morphology. The distributions are characterized by a single mode that shifts to smaller values as the pressing intensity increases.

Figure 1

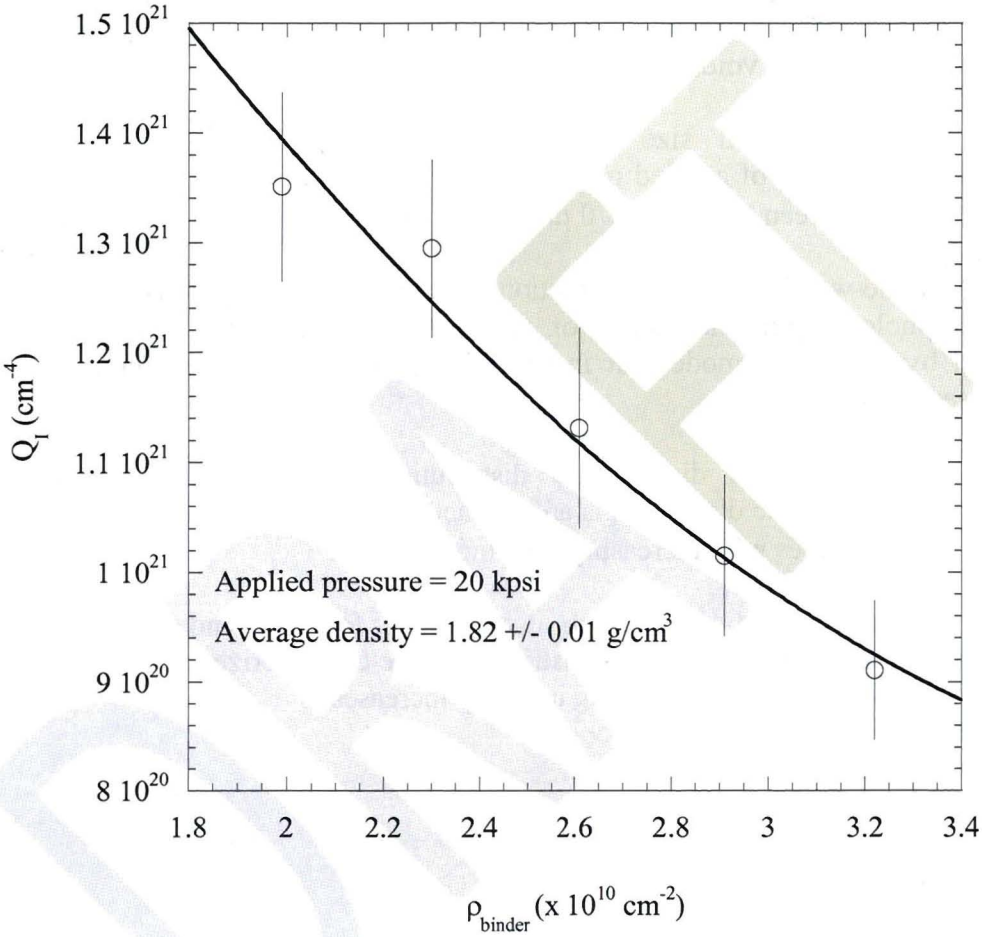
1.5 10^21
1.4 10^21
1.3 10^21
1.2 10^21
1.1 10^21
1 10^21
9 10^20
8 10^20
Q_l (cm^-4)
Applied pressure = 20 kpsi
Average density = 1.82 +/- 0.01 g/cm^3
1.8
2
2.2
2.4
2.6
2.8
3
3.2
3.4
ρ_binder (x 10^10 cm^-2)

Figure 2

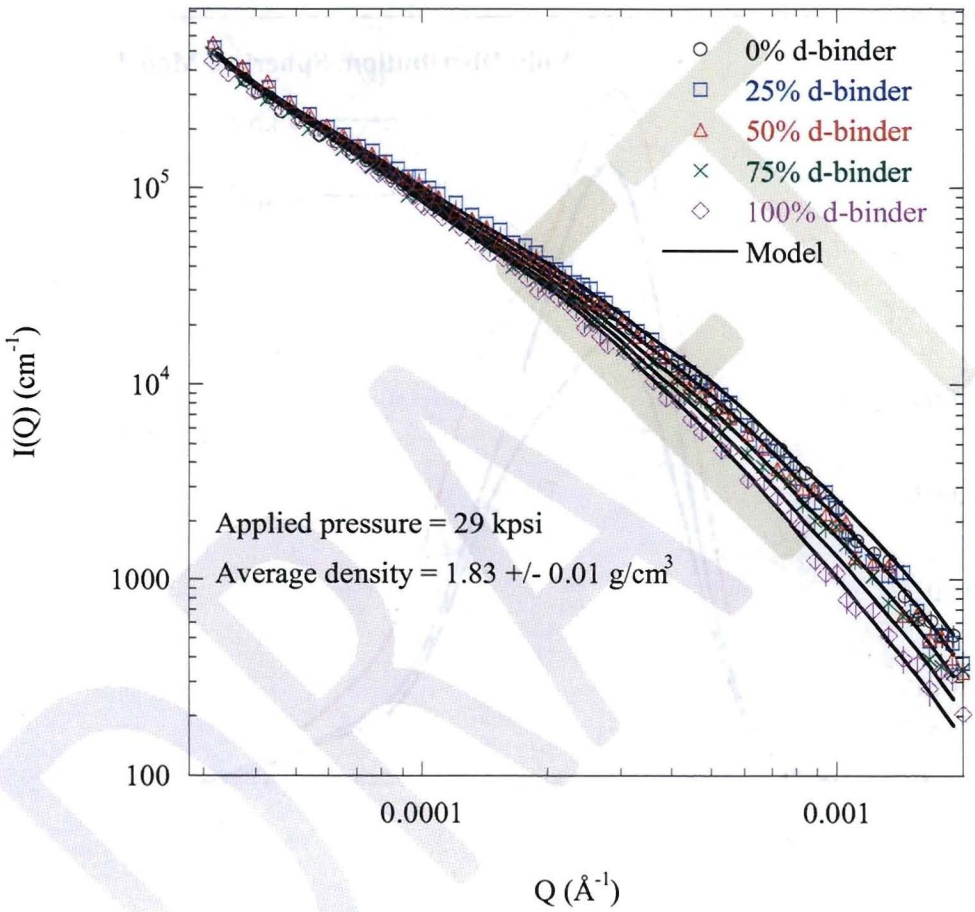
0% d-binder
25% d-binder
50% d-binder
75% d-binder
100% d-binder
Model
Applied pressure = 29 kpsi
Average density = 1.83 +/- 0.01 g/cm3
I(Q) (cm-1)
Q (Å-1)
10^5
10^4
1000
100
0.0001
0.001

Figure 3

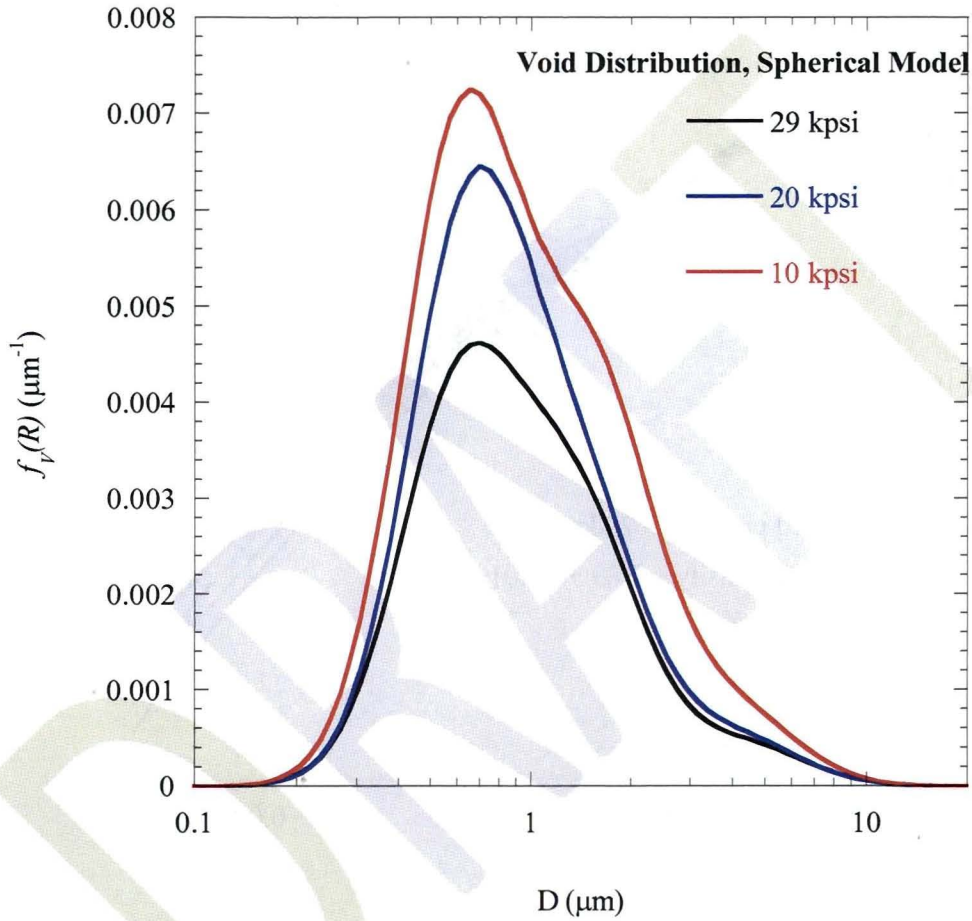
Void Distribution, Spherical Model
29 kpsi
20 kpsi
10 kpsi
0.008
0.007
0.006
0.005
0.004
0.003
0.002
0.001
0
0.1
1
10
$f_V(R)$ (μm^{-1})
D (μm)

Figure 4

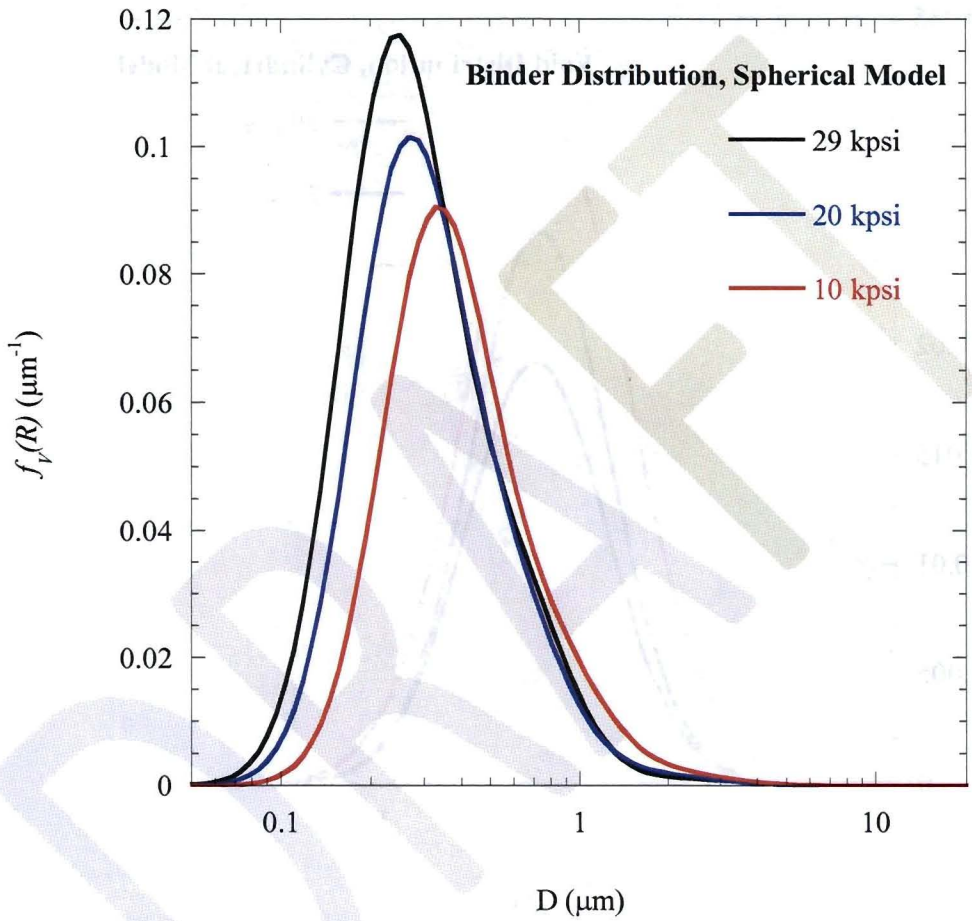
Binder Distribution, Spherical Model
29 kpsi
20 kpsi
10 kpsi
0.12
0.1
0.08
0.06
0.04
0.02
0
0.1
1
10
$f_v(R)$ (μm^{-1})
D (μm)

Figure 5

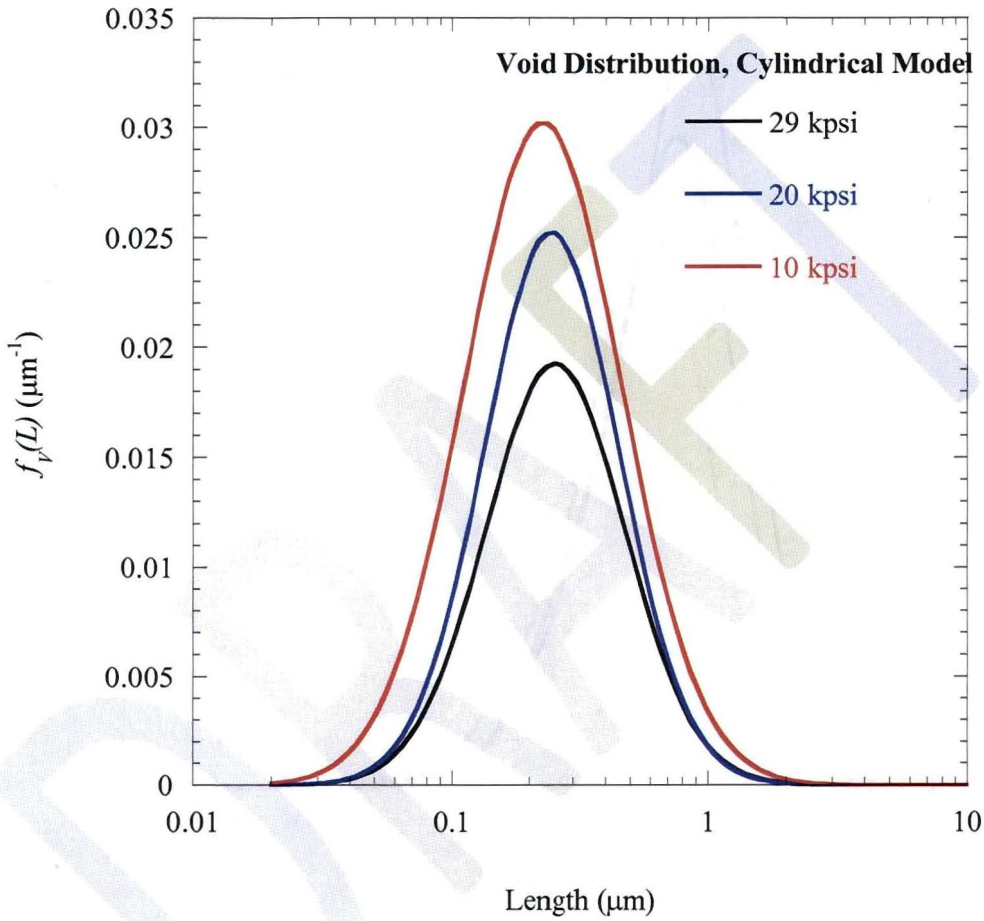
Void Distribution, Cylindrical Model
29 kpsi
20 kpsi
10 kpsi
0.035
0.03
0.025
0.02
0.015
0.01
0.005
0
0.01
0.1
1
10
$f_v(L)$ (μm^{-1})
Length (μm)

Figure 6